10th World Congress on Structural and Multidisciplinary Optimization
May 19 -24, 2013, Orlando, Florida, USA

A 3D topology optimization model of the cathode air supply channel in planar solid oxide fuel cell

Xiankai Song, Alejandro R Diaz, Andre Benard

Mechanical Engineering, Michigan State University, East Lansing, Michigan, USA, diaz@egr.msu.edu

1. Abstract
A 3D topology optimization model is developed to maximize the current generation of the cathode by designing the geometry of an air supply channel found in solid oxide fuel cells (SOFC). The problem is reduced to a periodic, coupled problem in consideration of a convection dominated oxygen gas transport in the air flow and oxygen ion diffusion in the solid cathode. The air flow field is calculated using a modified momentum equation with a Darcy flow term, and the result is used as a known parameter in the calculation of the oxygen gas transport. The oxygen gas transport is coupled with the oxygen ion diffusion by a design-dependent oxygen exchange boundary condition. Numerical examples discuss the effect of geometric parameters.

2. Keywords: solid oxide fuel cell, topology optimization, cathode design

3. Introduction
A SOFC converts chemical energy directly into electrical power and offers the considerable potential of a high efficiency and environmental friendly electrical power source [1]. Distinguished from other types of fuel cells, the oxygen ions migrate through a solid electrolyte for the completion of electrochemical reactions in the solid electrodes. The structure of a planar SOFC is illustrated in Figure 1.

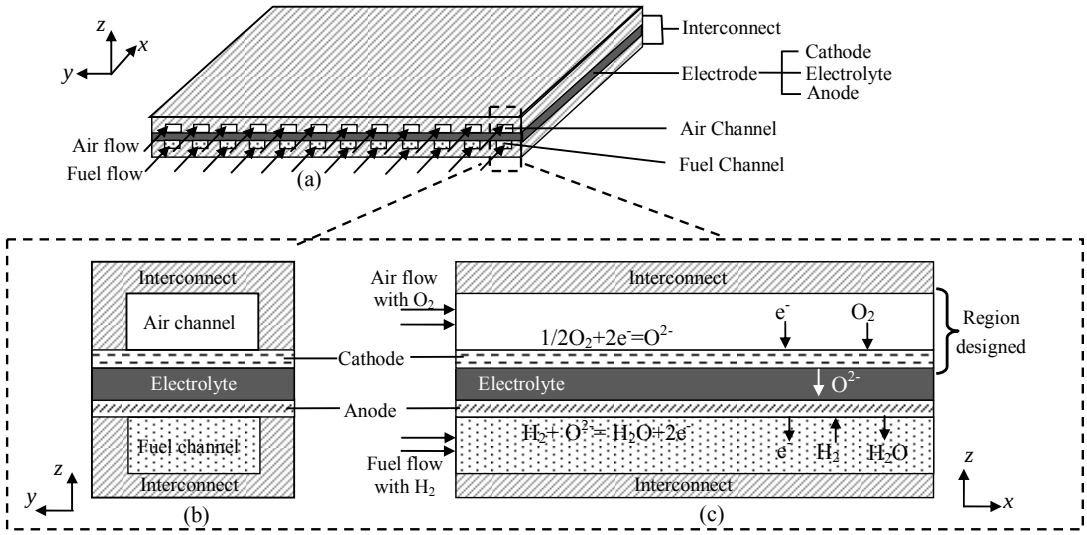

Figure 1: Schematic arrangement of a planar SOFC: (a) overview (b) front view (c) side view

In a SOFC, there are voltage losses associated with the ohmic resistances in the electrodes and the active polarizations on the air-cathode interface and the fuel-anode interface [2]. However, the voltage losses in a cathode usually dominate the entire stack so it is more efficient to focus on improving the cathode performance [3].Attempts in designing the cathode geometry from macro to micro scales have shown progresses in reducing the cathode resistance. Chan et al. [4] performed a sensitivity analysis for a generic macro-homogeneous polarization model of a solid oxide fuel cell to study the effect of the thickness of the fuel cell components. In a smaller scale, the advantage of using non-flat cathode-electrolyte interface is

explored based on a homogenized model of porous cathode (Iwai et al) [5]. Efforts have also been made in micro structure design. Shal et al. [6] deposited conductive electrocatalyst nano-particles of a mixed ionic electronic conducting (MIEC) material into a porous ionic-conducting scaffold to form a high performance SOFC composite cathode. Recently, Wang and Nicholas [7] proposed a simplified micro model of the composite cathode performance and applied it in a parametric design of the micro structure of the composite cathode. In addition, it is possible to improve performance by increasing the air/fuel supply by designing the air/fuel path. Huang et al. [8] studied the influence of flow uniformity in an array of channels by controlling the sizes of interconnects between the channels of SOFC. Kapadis et al. [9] computed the sensitivity of the anode performance in a 3D SOFC model, and presented a shape optimization of fuel channels. The effect of inserting rectangular pins transversely into air channel of a proton exchange membrane (PEM) was studied by Obayopo er al. [10], and the optimized geometric parameters of the pins were obtained.

Previous work by the authors [11] used a simplified 2D model to explore the effect of altering the shape of the microstructural features found in the cathode. Ignoring the oxygen gas transport around the microstructure, the model was reduced to a 2D oxygen ion diffusion problem with a design-dependent ionic transfer boundary condition. That simplification is only valid when oxygen gas supply is saturated.

In this work, a 3D topology optimization model is presented in consideration of both the cathode resistance and the air supply (the scale of the problem is different than in [11]). The current generation is maximized by altering the air flow path in a medium Reynolds number (1<Re<100), modifying the air-cathode interface (oxygen exchange interface) and adjusting the path of oxygen ion diffusion in the cathode. The air flow in the channel with design-dependent geometry is modeled using a Brinkman formulation of the momentum equation [12]. The resulting velocity field is used as a known parameter in the calculation of the oxygen gas transport. The oxygen gas transport is described by the convection-diffusion equation and is coupled with the oxygen ion diffusion by an oxygen exchange (ionic transfer) boundary condition. Although the 3D model can accommodate several design concepts, only two design strategies are explored in this work (discussed in Sec. 6), focusing on the concepts that are easier to manufacture.

4. Analysis model

Previous models of SOFC stacks have been proposed in [13, 14] and their results show that the oxygen consumption is low and the air flow is laminar with low pressure drop, so the air flow is assumed to be incompressible and independent with the oxygen gas transport. The low oxygen consumption also motivates the idea that a cathode structure with periodicity along the flow direction may achieve a balance between good performance and ease of manufacture. The length of the channel is assumed to be much larger than the size of the cross section, so the air flow becomes well developed in most of the channel, and the inlet and outlet effects can be neglected (the developing flow region is small compared to the channel length).

In this work, the analysis domain $\boldsymbol{\Omega}$ is selected to be a periodic unit of the rectangular air supply channel (shown in Figure 2). The solid cathode region $\boldsymbol{\omega}$ is an unknown sub-domain of $\boldsymbol{\Omega}$, and $\boldsymbol{\Omega}\backslash\boldsymbol{\omega}$ corresponds to the fluid region. The flow at the inlet boundary Γ_{in} and the flow at the outlet boundary Γ_{out} are considered to be periodic. The flow is driven by a prescribed pressure drop $\Delta p \leq 0$. To show the influence of the solid region to the flow field, porous media are distributed in the analysis domain. The regions with very low permeability block nearly all the flow through it as the solid cathode did, and the regions with very high permeability permit the flow to pass as in pure fluid. They indicate the solid cathode and the flow path, respectively. The flow field is governed by a Brinkman model [12] of steady-state Navier-Stokes equation with a Darcy flow term (in porous media) $\alpha(\xi)$, where ξ is the design variable distribution. $\xi = 0$ in $\boldsymbol{\omega}$ (solid), and $\xi = 1$ in $\boldsymbol{\Omega}\backslash\boldsymbol{\omega}$ (fluid).

$$-\nabla \cdot (\mu(\nabla \mathbf{u} + (\nabla \mathbf{u})^{\mathrm{T}}) - \mathbf{I}p) + \mathbf{u} \cdot \rho \nabla \mathbf{u} + \alpha(\xi)\mathbf{u} = 0 \qquad \text{in } \boldsymbol{\Omega} \tag{1}$$

where $\mathbf{u}$ is the velocity field, p is the pressure. The viscosity μ and the mass density ρ are constants in the analysis domain. A wall boundary condition (no slip) is applied on $\Gamma_{\text{w}} \cup \Gamma_0$

$$\mathbf{u} = 0 \quad \text{on } \Gamma_{\text{w}} \cup \Gamma_0 \tag{2}$$

and a periodic boundary condition is applied on Γ_{in} and Γ_{out}

$$\mathbf{u}(\boldsymbol{x}|\boldsymbol{x} \in \Gamma_{\text{in}}) = \mathbf{u}(\boldsymbol{x} + L\boldsymbol{e_x}|\boldsymbol{x} + L\boldsymbol{e_x} \in \Gamma_{\text{out}}) \qquad \text{on } \Gamma_{\text{in}} \text{ and } \Gamma_{\text{out}} \tag{3}$$

$$p(\boldsymbol{x}|\boldsymbol{x} \in \Gamma_{\text{in}}) + \Delta p = p(\boldsymbol{x} + L\boldsymbol{e_x}|\boldsymbol{x} + L\boldsymbol{e_x} \in \Gamma_{\text{out}}) \qquad \text{on } \Gamma_{\text{in}} \text{ and } \Gamma_{\text{out}} \tag{4}$$

where $\boldsymbol{x}$ is the spatial coordinate, L is the length of the periodic unit and $\boldsymbol{e_x}$ is the unit vector along the flow direction.

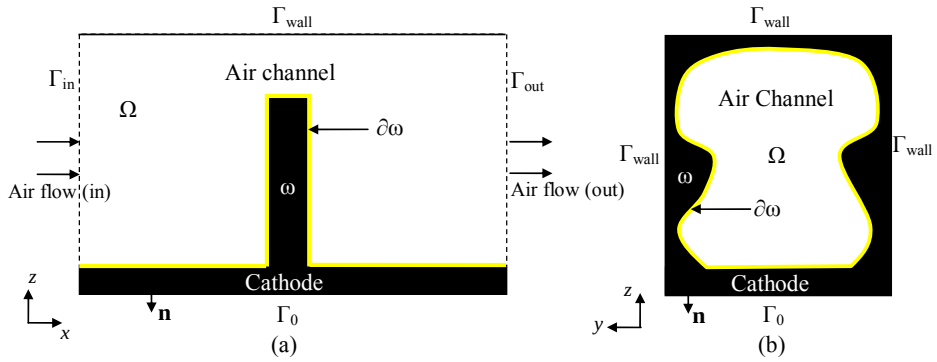

Figure 2: The analysis domain **Ω**: (a) side view (b) front view

Because the flow that penetrates into the nearly solid region (the porous cathode) is very small, and the diffusivity of oxygen gas in solid is also negligible compared to the diffusivity in fluid, the model of a convection diffusion equation with a design dependent oxygen gas diffusivity distribution is used to express the oxygen gas transport route around the solid cathode

$$\mathbf{u}\cdot\nabla c_{O_2}-\sigma(\xi)\nabla^2 c_{O_2}=0 \qquad \text{in } \boldsymbol{\Omega} \tag{5}$$

where c_{O_2} is the concentration of oxygen gas, and $\sigma(\xi)$ is the design dependent oxygen gas diffusivity which equals to σ_{O_2} when $\xi=1$ and has a very small value $\sigma_{\min}$ when $\xi=0$.

Standard air is pumped into the air channel, so the average concentration of the oxygen gas is constrained at the inlet

$$\frac{\int_{\Gamma_{in}} c_{O_2}\eta(\xi)d\Gamma_{in}}{\int_{\Gamma_{in}}\eta(\xi)d\Gamma_{in}}=c_0 \qquad \text{on } \Gamma_{in} \tag{6}$$

where c_0 is the standard concentration of oxygen gas in air and $\eta(\xi)$ is a geometric factor that indicates the area of the flow path at the inlet boundary. $\eta=1$ when $\xi=1$ and $\eta=0$ when $\xi=0$.

Given periodic cathode geometry and flow field, the oxygen gas transport can be expected to be periodic with an unknown small decay rate $\gamma\le 1$

$$\gamma c_{O_2}(\boldsymbol{x}|\boldsymbol{x}\in\Gamma_{in})=c_{O_2}(\boldsymbol{x}+L\boldsymbol{e_x}|\boldsymbol{x}+L\boldsymbol{e_x}\in\Gamma_{out}) \quad \text{on } \Gamma_{in} \text{ and } \Gamma_{out} \tag{7}$$

Supplied by the periodic oxygen gas transport, the oxygen ion diffusion is also assumed to be periodic with the same decay rate as the oxygen gas transport. The diffusion of the charged oxygen ion forms an ionic potential distribution, and it is described by Laplace's equation

$$-k(\xi)\nabla^2\phi=0 \qquad \text{in } \boldsymbol{\Omega} \tag{8}$$

where ϕ is the ionic potential and $k(\xi)$ is the design dependent oxygen ion diffusivity distribution in a opposite way to the oxygen gas transport case: $k(\xi)$ equals to $k_{O^{2-}}$ when $\xi=0$ and becomes a very small value $k_{\min}$ when $\xi=1$.

The oxygen ion diffusion is also assumed to be periodic with the decay rate γ, and the ionic potential is assigned to be zero at the bottom boundary Γ_0

$$\gamma\phi(\boldsymbol{x}|\boldsymbol{x}\in\Gamma_{in})=\phi(\boldsymbol{x}+L\boldsymbol{e_x}|\boldsymbol{x}+L\boldsymbol{e_x}\in\Gamma_{out}) \quad \text{on } \Gamma_{in} \text{ and } \Gamma_{out} \tag{9}$$

$$\phi=0 \qquad \text{on } \Gamma_0 \tag{10}$$

At the air-cathode interface $\partial\boldsymbol{\omega}$, the electrochemical reaction absorbs oxygen gas from the air and releases oxygen ion to the solid cathode, so it is modeled using a convection-like oxygen exchange boundary condition. The dependency of the ionic potential distribution and the current generation density can be treated ohmically at low current density [15],

$$i=\frac{\phi^{\infty}-\phi}{R_s} \qquad \text{on } \partial\boldsymbol{\omega} \tag{11}$$

where i is the current generation per unit area of $\partial\boldsymbol{\omega}$, ϕ^{∞} is the driving potential which comes from the Nernst voltage and R_s is the interface resistance, which can be expressed by [13][15]

$$R_s=\frac{\phi^{\infty}}{i_0} \tag{12}$$

$$i_0=\gamma_c\left(\frac{c_{O_2}}{c^{ref}}\right)^{0.25}\exp\left(\frac{-E_{act,c}}{RT}\right) \tag{13}$$

where γ_c is the cathodic pre-exponential coefficients, c^{ref} is the reference concentration, $E_{act,c}$ is the cathodic activation energy, R is the universal gas constant and T is the temperature. All of these quantities

are assumed to be constants.
For a small c_{O_2}/c^{ref} , Eq. (13) can be linearized for convenience of calculations, and Eqs. (11)-(13) can be simplified as

$$i = h_0(\phi^{\infty} - \phi)\, c_{O_2} \qquad \text{on } \partial\boldsymbol{\omega} \tag{14}$$

where h_0 is the oxygen exchange constant derived from eq. (11)-(13).
The corresponding oxygen gas loss is

$$Q = -\frac{h_0}{zq_e n_0}(\phi^{\infty} - \phi)\, c_{O_2} \qquad \text{on } \partial\boldsymbol{\omega} \tag{15}$$

where z is the particle charge of oxygen ion, q_e is the electron charge and n_0 is the Avogadro constant.

5. Finite element model and topology optimization problem

Aiming at maximizing the current output of the cathode, this work designs the geometry of the cathode and its air supply channel. The geometry of the cathode is described by the design variable field $\boldsymbol{\xi}$ which is relaxed to have any value between 0 (solid) and 1(fluid) to avoid dealing with the integer optimization problem. As discussed in Sec. 4, the whole cathode and its air supply channel is divided into a chain of periodic units, and the periodic unit is selected to be the analysis domain.
The analysis domain $\boldsymbol{\Omega}$ is discretized by 8 nodes rectangular element, and the air flow, the oxygen gas transport and the oxygen ion diffusion share the same mesh. However, the equal order interpolation of the velocity and pressure fields does not satisfy the Ladyzhenskaya-Babuška-Brezzi (LBB) condition for the flow problem, and this dissatisfaction forms numerical oscillation in pressure [12]. A SUPG stabilizer which penalizes large pressure gradient is introduced [16], and the stabilized matrices form of the flow equations (eq. (1)) is given as

$$\sum_e \begin{bmatrix} K^e_{NS}(\mathbf{u}) + K^e_D(\mathbf{u}, \boldsymbol{\alpha}^e(\xi^e)) & G^e_{NS}(\mathbf{u}) \\ L^e_{NS}(\mathbf{u}) & M^e_{NS}(\mathbf{u}) \end{bmatrix} \begin{pmatrix} \mathbf{u}^h \\ \boldsymbol{p}^h \end{pmatrix} = -\sum_e \begin{bmatrix} G^e_{NS}(\mathbf{u}) \\ M^e_{NS}(\mathbf{u}) \end{bmatrix} \Delta\boldsymbol{p} \qquad \text{in } \boldsymbol{\Omega} \tag{16}$$

where $\mathbf{u}^h$ and $\boldsymbol{p}^h$ belongs to suitable admissible spaces $\mathbf{V}^h_{\mathbf{u}}$ and $\mathbf{V}^h_{\boldsymbol{p}}$, respectively. $\Delta\boldsymbol{p}$ is the pressure drop vector which equals to Δp only on nodes located at Γ_{out}. K^e_{NS}, G^e_{NS}, L^e_{NS} and M^e_{NS} are the elemental stiffness matrices with the SUPG stabilizer for the Navier-Stokes flow, and K^e_D corresponds to the Darcy flow term in eq. (1).
The oxygen gas transport problem is coupled with the oxygen ion transport problem by the oxygen exchange boundary conditions (eq. (14)-(15)). They can also be extended to the intermediate design variable

$$i_{\partial e_j} = h^{\partial e}_j(\Delta\xi^e_j)(\phi^{\infty} - \phi)\, c_{O_2} \qquad \text{on } \partial e \tag{17}$$

$$Q_{\partial e_j} = -\frac{h^{\partial e}_j(\Delta\xi^e_j)}{zq_e n_0}(\phi^{\infty} - \phi)\, c_{O_2} \qquad \text{on } \partial e \tag{18}$$

where ∂e_j denotes the j_{th} surface of element e, $\Delta\xi^e_j$ is the difference of the design variable across ∂e_j, and $h^{\partial e}_j(\Delta\xi^e_j)$ are the design dependent oxygen exchange constants. If $\Delta\xi^e_j = 1$, $\partial e_j \in \partial\omega$ and $h^{\partial e}_j(\Delta\xi^e_j)$ equals to h_0.
The oxygen gas transport problem is convection dominated and it also needs to be stabilized. The matrices form equation of the couple problem (eq. (5) and eq. (8)) including SUPG stabilization [17] is

$$\sum_e \begin{bmatrix} K^e_{conv}(\mathbf{u}) + K^e_{diff}(\xi^e) + K^e_{stab}(\mathbf{u}, \xi^e) & 0 \\ 0 & K^e_{\phi}(\xi^e) \end{bmatrix} \begin{pmatrix} \mathbf{c}^h \\ \boldsymbol{\phi}^h \end{pmatrix} = \sum_{\partial e} \begin{bmatrix} Q^e(\mathbf{c}^h, \boldsymbol{\phi}^h, \Delta\xi^e_j) \\ I^e(\mathbf{c}^h, \boldsymbol{\phi}^h, \Delta\xi^e_j) \end{bmatrix} \quad \text{in } \boldsymbol{\Omega} \tag{19}$$

where $\mathbf{c}^h$ and $\boldsymbol{\phi}^h$ belongs to suitable admissible spaces $\mathbf{V}^h_{\mathbf{c}}$ and $\mathbf{V}^h_{\boldsymbol{\phi}}$, respectively. K^e_{conv}, $K^e_{diff}(\xi^e)$ and $K^e_{stab}(\mathbf{u}, \xi^e)$ are the elemental stiffness matrices of the convection, diffusion and stabilizer terms, respectively. K^e_{ϕ} is the elemental stiffness matrix of the oxygen ion diffusion. I^e and Q^e are the elemental oxygen exchange terms correspond to eq. (17)-(18), respectively.
To complete the topology optimization model, the interpolated function $\alpha(\xi)$ first proposed by Borrvall and Petersson [12] is used in the flow equations, and a SIMP-like approach [18] is used in a similar manner as the author's work [11] for a 2D problem associated with the cathode's microstructure design

$$\alpha^e(\xi^e) = \overline{\alpha} + (\underline{\alpha} - \overline{\alpha})\xi^e \frac{1+q}{\xi^e + q} \tag{20}$$

$$\sigma^e(\xi) = \sigma_{O_2}\xi^{e^r} + \sigma_{min}(1 - \xi^{e^r}) \tag{21}$$

$$\eta(\xi^e) = \xi^{e^r} \tag{22}$$

$$k^e(\xi^e) = k_{O^{2-}}(1 - \xi^{e^r}) + k_{min}\xi^{e^r} \tag{23}$$

$$h^{\partial e}_j(\Delta\xi^e_j) = \frac{h_0}{2}\left(\sqrt{\Delta\xi^{e^2}_j + \varepsilon^2} - \varepsilon\right)/\left(\sqrt{1 + \varepsilon^2} - \varepsilon\right) \tag{24}$$

where r is the penalty factor which is selected as 3, and ε is a small number to smoothen $h^{\partial e}_j(\Delta\xi^e_j)$ near $\Delta\xi^e_j = 0$, e.g. $\varepsilon = 0.001$.
A density filter with a linear weight [19] is used to prevent the appearance of checkerboard patterns and to

control feature size. A smoothed Heaviside projection function [20] is used to facilitate convergence to binary solutions.

$$\hat{\xi}_H^e = 1/2 + 1/2 \tanh\left(\beta\left(\hat{\xi}^e - 1/2\right)\right) / \tanh(\beta/2) \quad \textbf{(25)}$$

where $\hat{\boldsymbol{\xi}}^{\mathbf{e}}$ is the filtered design variable and β is a scaling factor that determines the sharpness of the projection.

The objective function is the total current generation of the whole cathode. The current generation of one periodic unit is the current flowed to $\boldsymbol{\Gamma_0}$ (the electrolyte)

$$f_p(c, \phi, \xi) = \int_{\Gamma_0} -k\nabla\phi \cdot \mathbf{n} d\Gamma_0 \quad (26)$$

Considering the decay ratio $\boldsymbol{\gamma}$ between the adjacent periodic units, if using $\mathbf{f_p}$ as the current generation of the first periodic cell, the current generation of the i_{th} periodic cell can be expressed as

$$f_p^i = f_p \gamma^{i-1} \quad (27)$$

Adding the current generation of all the periodic units together, the optimization problem can be stated as:

Find $\boldsymbol{\xi}$ that

$$\text{Maximize } f = \sum_{i=1}^{N_p} f_p \gamma^{i-1} = f_p \frac{\gamma^{N_p}-1}{\gamma-1} \quad (28)$$

Subject to

$$0 \le \xi^e \le 1, \; e=1, 2, 3, \dots, N \quad (29)$$

where $\mathbf{N_p}$ is the number of periodic units in the cathode and N is the number of elements.

6. Examples

The optimization model accommodates a variety of designs. To balance high performance and ease of manufacturing, two design strategies are selected and both of them assume the cross section of the design domain to be uniform. One strategy is to add a planar cathode barrier transversely in a rectangular cross sectional air channel and to design the geometry of the barrier; the other is to design the cross section of the channel. The design domain is 3D, but the design variables distribute only on the 2D cross section. In the examples below, the length of the channel is 100mm, and the material properties are consistent with the values reported in [6] [7].

6.1. Examples of adding cathode barrier in the channel

In this example the analysis domain $\boldsymbol{\Omega}$ is a rectangular domain of the size $2\text{mm(length)} \times 4\text{mm(width)} \times 2\text{mm(height)}$, and it is discretized by $20 \times 40 \times 20$ elements. The bottom layer of the elements is denoted by $\boldsymbol{\Omega}_b$ (Figure 3), and it is fixed to be cathode. The design domain $\boldsymbol{\Omega}_d$ is a portion of $\boldsymbol{\Omega}\backslash\boldsymbol{\Omega}_b$. The rest part $\boldsymbol{\Omega}\backslash(\boldsymbol{\Omega}_b \cup \boldsymbol{\Omega}_d)$ is denoted by $\boldsymbol{\Omega}_{fix}$, in which there can be some assigned geometries but they do not change with design. The length of the analysis domain is denoted by L, and the length of the design domain is marked as l (barrier thickness).

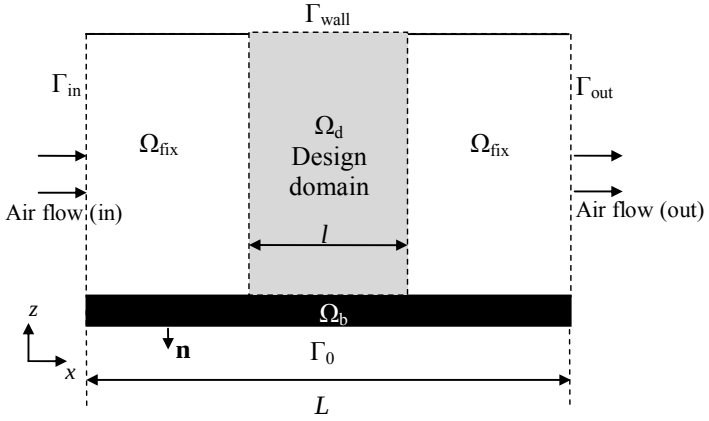

Figure 3: The design domain of example 1

Figure 4 and Table 1 show the effect of modifying the thickness l of the barrier on the geometry, and the performances of the optimized designs are compared with the performance of a reference design (Fig. 4(e)).

Oxygen gas transport in the air flow interacts with oxygen ion diffusion in the solid cathode to find a balance between sufficient air flow and large oxygen exchange (ionic transfer) interface. The designs (a)-(d) all have a ring-like shape to form a large interface area and keep a clear flow path in the center. The performance of a medium *l/L* value (Fig. 4(b)-(c)) is better than a very thin barrier (Fig. 4(a)) or a very thick barrier (Fig. 4(d)).

By increasing *l/L*, the total interface area is enlarged by generating more side faces of the barrier, but the total volume air flow becomes smaller in thicker barriers (Tab. 1). From Fig. 4(a) to Fig. 4(d), the designs become more emphasized on maintaining the total volume air flow, so the cross section areas of the flow paths rises from (a) to (d).

Detailed designs are also made in Fig. 4(a)-(d) to obtain more interface areas. The interface area of a barrier consists of two portions: one is the area on the front and back faces; the other is the area at the side face. For a thin barrier such as Fig. 4(a), the first portion dominates. The second portion takes the first place as the thickness increases, and small holes (Fig. 4(b), (c)) and wavy profile (Fig. 4(d)) are generated.

The current (carried by oxygen ion) generated by the cathode flows to the bottom, and the ohmic resistance in the cathode may impedes the current. Therefore, the designs need to ensure a low resistance path to the bottom. Because the current flow is accumulated to be larger near the bottom, the designs in Fig. 4(a)-(d) all become wider near the bottom, and the holes in Fig. 4(b) (c) are all generated far from the bottom.

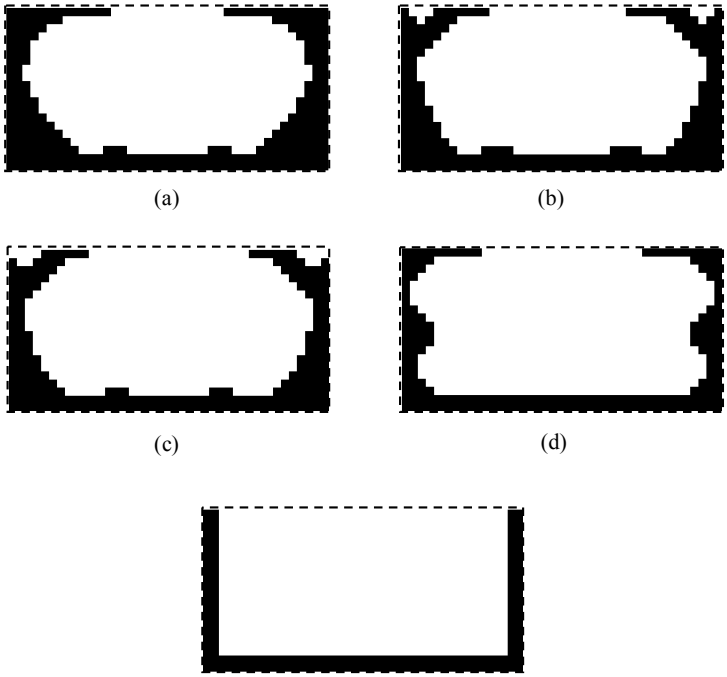

Figure 4: Optimized design for different *l/L* (a) 0.2 (b) 0.3 (c) 0.5 (d) 1.0 (e) reference design

Table 1: Performances of optimized designs for different *l/L*

l/L	Total volume air flow(m^3/sec)	f (A)	f_{ref}(A)	Improvement (%)
0.2	7.3e-6	1.64	1.52	8%
0.3	6.9e-6	1.69	1.55	9%
0.5	6.6e-6	1.76	1.61	9%
1.0	6.2e-6	1.68	1.55	8%

Fixing a non-electrochemical reactive pin transversely in $\boldsymbol{\Omega}_{fix}$, the change in flow paths will have a influence on the designs. A pin as shown in Figure 6(a) is inserted into $\boldsymbol{\Omega}_{fix}$ at the location $0.2L$ upstream of $\boldsymbol{\Omega}_{d}$ (as shown in Figure 5).

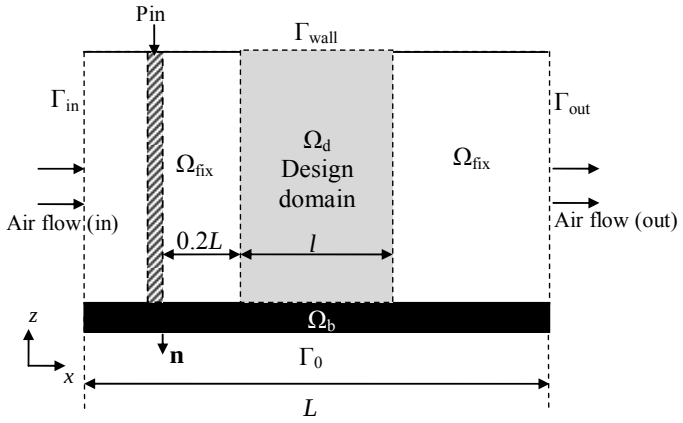

Figure 5: The design domain with the pin

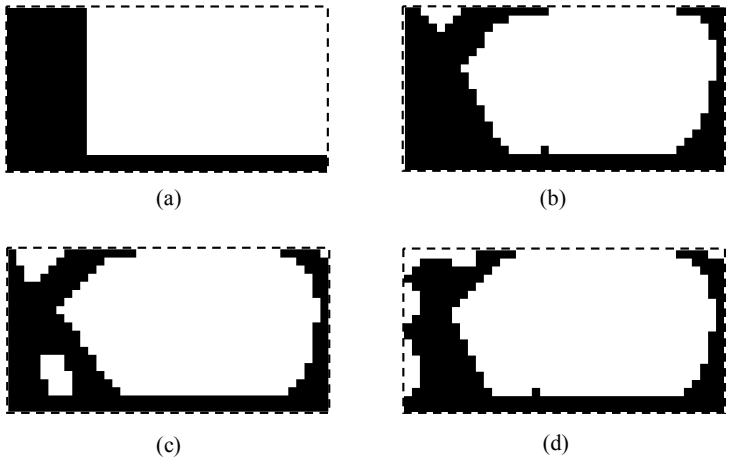

Figure 6: The shape of the pin (a) and the optimized design for different *l*/*L* (b) 0.2 (c) 0.3 (d) 0.5

Table 2: Performances of optimized designs with a fix pin in upstream for different *l*/*L*

l/*L*	f (A)	Total volume air flow(m^3/sec)
0.2	1.59	6.2e-6
0.3	1.64	5.9e-6
0.5	1.72	5.7e-6

Because the pin blocks 1/4 of the cross section of the analysis domain, both the total volume air flows and the performances (Tab. 2) of the designs Fig. 6(b)-(d) drop down than the corresponding designs Fig. 4(a)-(c). The locations of the flow paths in the barriers coincide with the flow path on the pin, and there are still small holes generated on the barriers to enlarge interface areas in the same manner with the designs in Fig. 4. However, because of the flow is blocked by the pin in the left 1/4 region, the oxygen supply dominates the design in this region, and the holes in this region (left 1/4 of the barrier) becomes larger and closer to the bottom.

6.2. Examples of designing the cross section of the channel

In this example the analysis domain $\boldsymbol{\Omega}$ is a rectangular domain of the size $0.4\text{mm(length)} \times 4\text{mm(width)} \times \text{H(height)}$, and it is arranged in the same way as shown in Fig. 3. The design domain $\boldsymbol{\Omega}_d$ spans the whole length of $\boldsymbol{\Omega}$, and $\boldsymbol{\Omega}_{fix} = \emptyset$. Figure 7 and Table 4 show the designs and

their performances with different H.

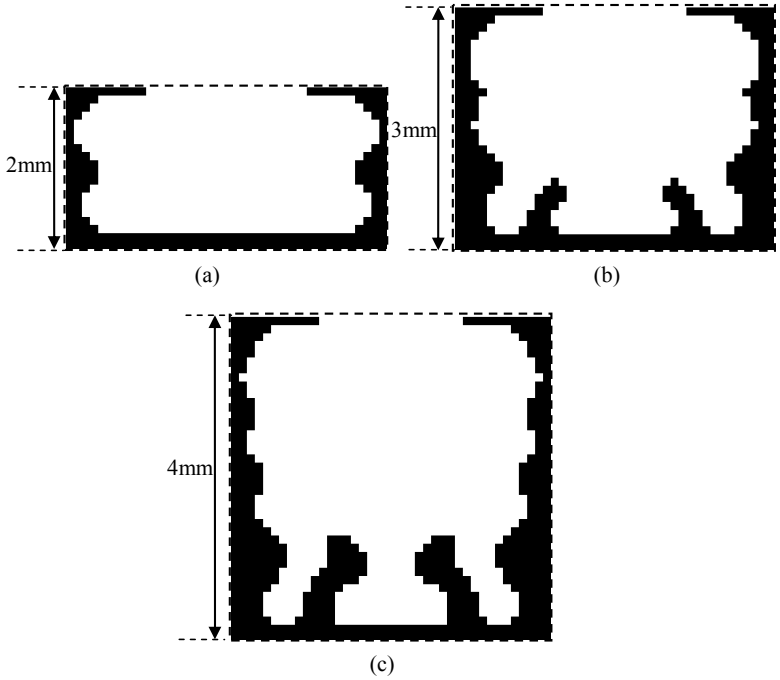

Figure 7: The optimized design for different H (a) 2.0mm (b) 3.0mm (c) 4.0mm

Table 4: Performances of optimized designs with different analysis domain sizes

H(mm)	f (A)	Total volume air flow(m^3/sec)	$\frac{f}{H}$ ($A \cdot sec/m^3$)
2.0	1.68	6.1e-6	0.84
3.0	2.64	11.2e-6	0.88
4.0	3.26	18.2e-6	0.81

By using a higher H, the air supply (volume air flow) becomes abundant, and the designs can afford to generate hedges to enlarge the interface areas. The hedges are generated near the bottom to ensure a low resistance path to the bottom. The current generation f can be enhanced by using a larger H. However, the size of a SOFC stack is also important in SOFC applications [2], and if fixing the Length and Width of the analysis domain, the current generation versus the channel size can be expressed by the ratio $\mathbf{f/H}$ (Shown in Tab. 4). The results in Tab. 4 shows in this case H=3mm is the optimal height.

7. Conclusions

A 3D coupled topology optimization model is presented to identify the optimized geometry of SOFC cathode in the air supply channel. The study points to the understanding of fluid-convection-diffusion interactions and their effect to the cathode performance. The optimized results provided show that a good design must achieve a balance between sufficient air supply, large oxygen exchange interface area and the ohmic resistance. The designs provided in this work show that the current generated can be increased by as much as nine percent and such designs can serve as references to help improving SOFC cathode design.

8. References

[1] Adler SB (2004) Factors governing oxygen reduction in solid oxide fuel cell cathodes. Chem Rev 104:4791–4843

[2] O'Hayre RP, Cha SW, Colella WG, Prinz FB (2009) Fuel cell fundamentals. Wiley, New York, pp 270–272

[3] Li XG (2006) Principles of fuel cells, Taylor Francis, New York, pp 494–503

[4] Chan SH, Khor K, Xia ZT (2001) A complete polarization model of a solid oxide fuel cell its sensitivity to the change of cell component thickness. J Power Sources 93:130–140
[5] Iwai H, Kuroyanagi A, Saito M, Konno A, Yoshida H, Yamada T, Nishiwaki S (2011) Power generation enhancement of solid oxide fuel cell by cathode-electrolyte interface modification in mesoscale assisted by level set-based optimization calculation. J Power Sources 196:3485–3495
[6] Shah M, Nicholas JD, Barnett SA (2009) Prediction of infiltrated solid oxide fuel cell cathode polarization resistance using simple models. Electrochem Commun 11:2–5
[7] Wang L, Nicholas JD (2011) Simple Infiltrated Microstructure Polarization Loss Estimation (SIMPLE) model predictions of today tomorrow's nano-composite SOFC cathodes. In: Singhal S, Eguchi K (eds) Twelfth international symposium on solid oxide fuel cells, pp 2321–2329 (ECS Transactions, The Electrochemical Society, Montreal, Canada, 2011)
[8] Huang CM, Shy SS, Lee CH (2008) On flow uniformity in various interconnects and its influence on cell performance of planar SOFC. J Power Sources 183:205-213
[9] Kapadia S, Anderson WK, Burdyshaw C (2011) Channel shape optimization of solid oxide fuel cells using advanced numerical techniques, Computers & Fluids 41:41-50
[10] Obayopo SO, Bello-Ochende T, Meyer JP (2012) Modeling and optimization of reactant gas transport in a PEM fuel cell with a transverse pin fin insert in channel flow, Int. J. Hydrogen Energy 37: 286-298
[11] Song X, Diaz AR, Benard A, Nicholas JD (2012) A 2D model for shape optimization of solid oxide fuel cell cathodes, Struct Multidisc Optim 44:19–24
[12] Borrvall T, Peterson J (2003) Topology optimization of fluids in Stokes flow, Int. J Numerical methods in Fluids 41(1): 77-108
[13] Costamagna P, Honegger K (1998) Modeling of solid oxide heat exchanger integrated stacks and simulation at high fuel utilization, J. Electrochem. Soc. 145(11): 3995-4007
[14] Akhtar N, Decent SP, Loghin D, Kendall K (2009) A three-dimensional numerical model of a single-chamber solid oxide fuel cell, Int. J Hydrogen Energy 34: 8645-8663
[15] Tanner CW, Fung KZ, Virkar AV (1997) The effect of porous composite electrode structure on solid oxide fuel cell performance: theoretical analysis. J Electrochem Soc 144(1): 21–30
[16] Tezduyar TE, Mittal S, Ray SE, Shih R (1992) Incompressible flow computations with stabilized bilinear and linear equal –order-interpolation velocity-pressure elements, Comp. Meth. Appl. Mech. Engng. 95: 221-242
[17] Brooks AN, Hughes TJR (1982) Streamline upwind/Petrov-Galerkin formulations for convection dominated flows with particular emphasis on the incompressible Navier-Stokes equations. Comp. Meth. Appl. Mech. Engng. 32(1-3):199-259
[18] Bendsøe MP (1989) Optimal shape design as a material distribution problem. Struct Optim 1(4):193–202
[19] Sigmund O, Petersson J (1998) Numerical instabilities in topology optimization: a survey on procedures dealing with checkboards, mesh dependencies local minima. Struct Optim 16: 68–75
[20] Kawamoto A, Matsumori T, Yamasaki S, Nomura T, Kondoh T, Nishiwaki S (2011) Heaviside projection based topology optimization by a PDE-filtered scalar function. Struct Multidisc Optim 44:19–24